Seismic attenuation compensation via inversion and imaging

Yufeng Wang

Stanford Wave Physics Lab

Stanford University

Nov 30, 2018

Outline

Motivation
L_{1-2} minimization for seismic attenuation compensation
- Nonstationary convolution model
- Inversion-based compensation
- Solver for L_{1-2} minimization
- Examples

Adaptive stabilization for Q-ARTM and Q-ERTM
- Constant-Q wave equation and k-space Green's function
- Adaptive stabilization
- From viscoacoustic to viscoelastic
- Examples

High performance computing and code packages
- Reproducible research
- Architecture of cu$Q$-RTM code package
- Speedup and scaling

Summary

Applications

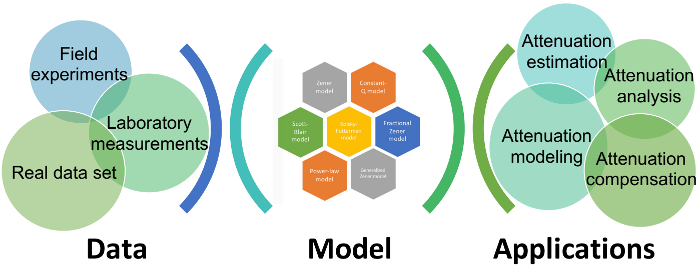

Background

- Amplitude absorption and phase distortion degrade the quality of seismograms, decrease the resolution of migrated images and eventually affect the reliability of seismic interpretation.
- In general, attenuation compensation in geophysics can be roughly classified into two categories: seismic record-based compensation and propagation-based compensation.

Motivation

- Inversion-based compensation enjoys better stability over traditional inverse Q filtering. However, constrained L_1 minimization serving as the convex relaxation of the literal L_0 sparsity count may not give the sparsest solution[1].
- Recently, nonconvex metric for compressed sensing has attracted considerable research interest[2]. We propose a nearly unbiased approximation of the vector sparsity, denoted as L_{1-2} minimization, for exact and stable seismic attenuation compensation.

---

[1] Tian-Hui Ma, Yifei Lou, and Ting-Zhu Huang. "Truncated l_1-2 Models for Sparse Recovery and Rank Minimization". In: *SIAM Journal on Imaging Sciences* 10.3 (2017), pp. 1346–1380.

[2] Emmanuel J Candes, Michael B Wakin, and Stephen P Boyd. "Enhancing sparsity by reweighted ℓ_1 minimization". In: *Journal of Fourier analysis and applications* 14.5 (2008), pp. 877–905.

Motivation

- Amplitude attenuation and phase dispersion associated with anelasticity occur during the wave propagation, so it is more physically consistent to mitigate these effects in a prestack depth migration[3][4].
- Amplitude compensation is prone to boost high-frequency noise in seismic data or the machine errors relative to working precision. We develop an adaptive stabilization scheme for Q-ARTM and Q-ERTM, which exhibits the superior properties of time-variance and Q-dependence over conventional low-pass filtering.

[3] Yu Zhang, Po Zhang, and Houzhu Zhang. "Compensating for visco-acoustic effects in reverse-time migration". In: *SEG expanded abstracts: 80th Annual international meeting*. 2010, pp. 3160–3164.

[4] Tieyuan Zhu, Jerry M. Harris, and Biondo Biondi. "Q-compensated reverse-time migration". In: *Geophysics* 79.3 (2014), S77–S87.

Outline

Motivation
L_{1-2} minimization for seismic attenuation compensation
- Nonstationary convolution model
- Inversion-based compensation
- Solver for L_{1-2} minimization
- Examples

Adaptive stabilization for Q-ARTM and Q-ERTM
- Constant-Q wave equation and k-space Green's function
- Adaptive stabilization
- From viscoacoustic to viscoelastic
- Examples

High performance computing and code packages
- Reproducible research
- Architecture of cu$Q$-RTM code package
- Speedup and scaling

Summary

Kolsky-Futterman model

Kolsky (1956) and Futterman (1962) assumed that frequency-dependent attenuation coefficient $\alpha(\omega)$ is strictly linear with frequency over the range of measurement:[5][6]

$$\frac{1}{c_p(\omega)} = \frac{1}{c_p(\omega_0)}\left(1 - \frac{1}{\pi Q(\omega_0)}\ln\left|\frac{\omega}{\omega_0}\right|\right), \tag{1}$$

where $c_p(\omega_0)$ and $Q(\omega_0)$ are the values of the phase velocity and approximate Q at the reference frequency ω_0.

[5] H Kolsky. "LXXI. The propagation of stress pulses in viscoelastic solids". In: *Philosophical magazine* 1.8 (1956), pp. 693–710.

[6] Walter I Futterman. "Dispersive body waves". In: *Journal of Geophysical research* 67.13 (1962), pp. 5279–5291.

Modified Kolsky-Futterman model

Wang and Guo (2004) pointed out that the phase velocity formula 1 is merely an asymptotic formula for $\omega \gg \omega_0$.[7] As exploration seismic data have relative low frequency range within $10^0 - 10^2$ Hz, they therefore proposed a modified Kolsky-Futterman model as follows:

$$\frac{1}{c_p(\omega)} = \frac{1}{c_p(\omega_0)}\left(1 - \frac{1}{\pi Q(\omega_0)}\ln\left|h\frac{\omega}{\omega_0}\right|\right) \approx \frac{1}{c_p(\omega_0)}\left|\frac{\omega}{\omega_h}\right|^{-\gamma}, \qquad (2)$$

where the dimensionless parameter $\gamma = \frac{1}{\pi Q(\omega_0)}$ and ω_h is a redefined tuning parameter.

[7] Yanghua Wang and Jian Guo. "Modified Kolsky model for seismic attenuation and dispersion". In: *Journal of Geophysics & Engineering* 1.3 (2004), p. 187.

Modified Kolsky-Futterman model

The complex wavenumber of Modified Kolsky-Futterman model:

$$k(\omega) = \frac{\omega}{c_p(\omega_0)} \left| \frac{\omega}{\omega_h} \right|^{-\gamma} \left(1 - \frac{i}{2Q(\omega)} \right). \tag{3}$$

Substituting the complex wavenumber $k(\omega)$ into the plane wave expression, we have

$$\begin{aligned} p(\mathbf{x}, t) &= e^{i\left[\omega t - \frac{\omega}{c_p(\omega_0)} \left| \frac{\omega}{\omega_h} \right|^{-\gamma} \left(1 - \frac{i}{2Q(\omega)}\right) \mathbf{x}\right]} \\ &= e^{i\omega t} e^{-i \frac{\omega}{c_p(\omega_0)} \left| \frac{\omega}{\omega_h} \right|^{-\gamma} \mathbf{x}} e^{-\frac{\omega}{2 c_p(\omega_0) Q(\omega)} \left| \frac{\omega}{\omega_h} \right|^{-\gamma} \mathbf{x}}. \end{aligned} \tag{4}$$

Modified Kolsky-Futterman model

We first replace the distance $\mathbf{x}$ with the traveltime $\tau = \frac{\mathbf{x}}{c_p(\omega_0)}$, and then define the following attenuation function

$$\begin{aligned} a(\omega,\tau) &= e^{i\omega\tau\left(1-\left|\frac{\omega}{\omega_h}\right|^{-\gamma}\right)} e^{-\frac{\omega\tau}{2Q(\omega)}\left|\frac{\omega}{\omega_h}\right|^{-\gamma}} \\ &\approx e^{i\omega\tau\left(1-\left|\frac{\omega}{\omega_h}\right|^{-\gamma}\right)} e^{-\frac{\omega\tau}{2Q(\omega_0)}\left|\frac{\omega}{\omega_h}\right|^{-\gamma}}, \end{aligned} \tag{5}$$

where the two exponential terms dominate phase dispersion and amplitude attenuation, respectively.

Nonstationary convolution model

The formula for nonstationary convolution model in the frequency domain can be described as follows:

$$s(\omega) = w(\omega) \int_0^T a(\omega, \tau) r(\tau) e^{-i\omega\tau} d\tau, \tag{6}$$

which can be discretized into a matrix-vector form:

$$\mathbf{s} = \mathbf{W}\mathbf{A}\mathbf{r}, \tag{7}$$

where the kernel matrix $\mathbf{W}$ represents the wavelet's band-pass filtering effects and matrix $\mathbf{A}$ stands for the earth's Q filtering effects.

Two-step compensation scheme

The frequency-domain discrete expression of the equation 7 gives the following close-form expression:

$$\begin{bmatrix} w(\omega_1)a(\omega_1,\tau_1)e^{-i\omega_1\tau_1} & \dots & w(\omega_1)a(\omega_1,\tau_T)e^{-i\omega_1\tau_T} \\ \vdots & \ddots & \vdots \\ w(\omega_L)a(\omega_L,\tau_1)e^{-i\omega_L\tau_1} & \dots & w(\omega_L)a(\omega_L,\tau_T)e^{-i\omega_L\tau_T} \end{bmatrix} \begin{bmatrix} r_1 \\ \vdots \\ r_T \end{bmatrix} = \begin{bmatrix} s(\omega_1) \\ \vdots \\ s(\omega_L) \end{bmatrix}. \tag{8}$$

The compensated seismic records can be obtained by convolut-ing a wavelet, i.e.,

$$\chi = \mathbf{W}\mathbf{r} = \mathbf{W}\mathbf{A}^{-1}\mathbf{W}^{-1}\mathbf{s}. \tag{9}$$

Instead of solving for χ using equation 9 directly, we perform seismic attenuation compensation via a two-step scheme.

Two-step compensation scheme

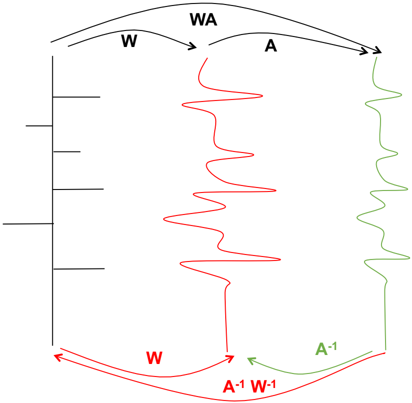

Figure 1. The diagram of the direct and two-step compensation processes, where the green line represents direct compensation method using $\mathbf{A}^{-1}$, the red lines stand for two-step compensation scheme using opertors $\mathbf{A}^{-1}\mathbf{W}^{-1}$ and $\mathbf{W}$.

Inversion with L_1 constraint

Inversion-based compensation in the frequency domain can be achieved by defining the following cost function with L_1 norm:

$$\min_{\mathbf{r}} \ \frac{1}{2} \|\mathbf{\Phi r} - \mathbf{s}\|_2^2 + \lambda \|\mathbf{r}\|_1 , \tag{10}$$

where the kernel matrix $\mathbf{\Phi} = \mathbf{WA}$ responsible for both the wavelet's band-pass filtering effects and the earth's Q filtering effects. The matrix $\mathbf{\Phi}$ can be considered as sensing matrix, which is required to satisfy the restricted isometry property (RIP) with small restricted isometry constants[8].

[8] Emmanuel J Candes and Terence Tao. "Decoding by linear programming". In: *IEEE transactions on information theory* 51.12 (2005), pp. 4203–4215.

RIP examination

It is generally NP-hard to verify whether $\mathbf{\Phi}$ is a RIP matrix or not[9]. Alternative way to predict RIP of $\mathbf{\Phi}$ is the so-called coherence, which is closely related to the RIP yet easy to examine[10].

$$\mu_{\mathbf{\Phi}}(i,j) := \frac{\left|\mathbf{\Phi}_i^T \mathbf{\Phi}_j\right|}{\left\|\mathbf{\Phi}_i\right\|_2 \left\|\mathbf{\Phi}_j\right\|_2}, \qquad i \neq j, \tag{11}$$

where $\mathbf{\Phi}_i$ and $\mathbf{\Phi}_j$ are arbitrary two columns from $\mathbf{\Phi}$.

[9] Afonso S. Bandeira et al. “Certifying the Restricted Isometry Property is Hard”. In: *IEEE Transactions on Information Theory* 59.6 (2013), pp. 3448–3450.

[10] D. L. Donoho and X. Huo. “Uncertainty principles and ideal atomic decomposition”. In: *IEEE Transactions on Information Theory* 47.7 (2002), pp. 2845–2862.

RIP examination

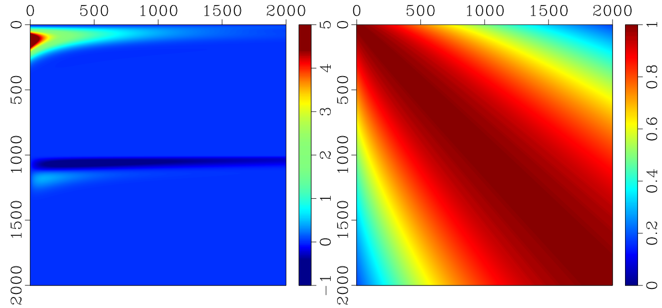

Figure 2. Visualization of (a) the frequency-domain matrix $\mathbf{\Phi}$ and (b) its coherence coefficients.

RIP examination

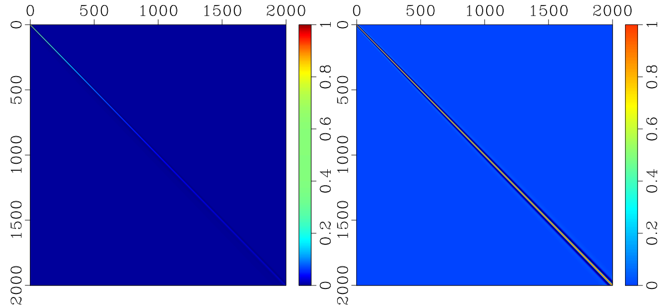

Figure 3. Visualization of (a) the time-domain matrix $\hat{\mathbf{\Phi}}$ and (b) its coherence coefficients.

Time-domain inversion

As frequency-domain sensing matrix $\mathbf{\Phi}$ exhibits high coherence, thus resulting in degraded inversion performance, we reformulate a new misfit function by transforming frequency-domain formula 10 into the time domain, and we have

$$\min_{\mathbf{r}} \; \frac{1}{2}\left\|\hat{\mathbf{\Phi}}\mathbf{r} - \hat{\mathbf{s}}\right\|_2^2 + \lambda \left\|\mathbf{r}\right\|_1 , \tag{12}$$

where the new kernel matrix $\hat{\mathbf{\Phi}}$ is obtained by transforming $\mathbf{\Phi}$ into time domain and reshaping it as a diagonal matrix form.

Nonconvex metrics

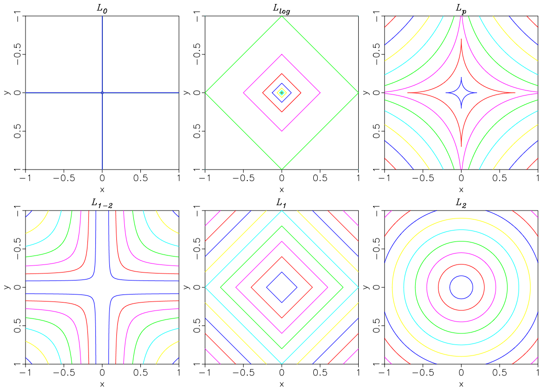

Figure 4. Contours of different penalties: (a) L_0, (b) L_{log} (LSP), (c) L_p $(p = 0.5)$, (d) L_{1-2}, (e) L_1 and (f) L_2.

Inversion with L_{1-2} constraint

We incorporate L_{1-2} metric into the inversion-based compensation scheme, the misfit function with L_{1-2} minimization is given as follows[11]

$$\min_{\mathbf{r}} \frac{1}{2} \left\| \hat{\mathbf{\Phi}}\mathbf{r} - \hat{\mathbf{s}} \right\|_2^2 + \lambda(\|\mathbf{r}\|_1 - \alpha \|\mathbf{r}\|_2), \tag{13}$$

where the weighted parameter α with the range of $[0, 1]$ is provided to deal with ill-conditioned matrices when L_{1-2} fails to obtain a good solution[12].

[11] Yufeng Wang et al. "L1-2 minimization for exact and stable seismic attenuation compensation". In: *Geophysical Journal International* 213.3 (2018), pp. 1629–1646.

[12] Yifei Lou, Stanley Osher, and Jack Xin. "Computational Aspects of Constrained L1-L2 Minimization for Compressive Sensing". In: *Petroleum Science & Technology* 23.1 (2015), pp. 47–54.

DCA

For the convenience and simplicity of formulas' deducing, we rewrite equation 13 as the following uniform formula:

$$\min_{x} \ \frac{1}{2} \left\| Ax - b \right\|_2^2 + \lambda(\left\| x \right\|_1 - \alpha \left\| x \right\|_2), \tag{14}$$

with $A = \hat{\mathbf{\Phi}}$, $x = \mathbf{r}$ and $b = \hat{\mathrm{s}}$. The DCA is an robust and efficient descent method to cope with the minimization of an objective function $F(x) = G(x) - H(x)$, where $G(x)$ and $H(x)$ are proper convex functions[13]. It gives

$$\begin{cases} y^k \in \partial H(x^k), \\ x^{k+1} = \arg\min_{x \in \mathbb{R}^n} \ G(x) - \left(H(x^k) + \langle y^k, x - x^k \rangle \right). \end{cases} \tag{15}$$

[13] Pham Dinh Tao and Le Thi Hoai An. "A DC optimization algorithm for solving the trust-region subproblem". In: *SIAM Journal on Optimization* 8.2 (1998), pp. 476–505.

DCA

The objective in 14 has the following convex decomposition

$$F(x) = \left(\frac{1}{2}\left\|Ax - b\right\|_2^2 + \lambda\left\|x\right\|_1\right) - \alpha\lambda\left\|x\right\|_2, \tag{16}$$

where $-\alpha\lambda\left\|x\right\|_2$ is differentiable with gradient

$$y^k = \begin{cases} \mathbf{0}, & if\ x^k = \mathbf{0}, \\ -\alpha\lambda\frac{x^k}{\left\|x^k\right\|_2}, & otherwise. \end{cases} \tag{17}$$

According to DCA iteration 15, L_{1-2} minimization 16 can be solved by the following scheme:

$$x^{k+1} = \arg\min_{x\in\mathbb{R}^n} \frac{1}{2}\left\|Ax - b\right\|_2^2 + \lambda\left\|x\right\|_1 + \langle y^k, x\rangle. \tag{18}$$

ADMM

The trick of ADMM formula is to decouple the coupling between the quadratic term and L_1 penalty by introducing an auxiliary variable z, equation 18 is equivalent to the following constrained minimization problem:

$$x^{k+1} = \arg\min_{x \in \mathbb{R}^n} \frac{1}{2} \|Ax - b\|_2^2 + \langle y^k, x \rangle + \lambda \|z\|_1 \text{ subject to } x - z = \mathbf{0}. \tag{19}$$

The augmented Lagrangian can be expressed as

$$\mathcal{L}_\rho(x, z, w) = \frac{1}{2} \|Ax - b\|_2^2 + \langle y^k, x \rangle + \lambda \|z\|_1 + w^T (x - z) + \frac{\rho}{2} \|x - z\|_2^2, \tag{20}$$

where y is the Lagrangian multiplier, ρ is the penalty parameter.

ADMM

The unscaled-form ADMM consists of the iterations[14][15]:

$$\begin{cases} z^{l+1} = \arg\ \min_z\ \mathcal{L}_\rho(x^l, z, w^l), \\ x^{l+1} = \arg\ \min_x\ \mathcal{L}_\rho(x, z^{l+1}, w^l), \\ w^{l+1} = w^l + \rho(x^{l+1} - z^{l+1}), \end{cases} \tag{21}$$

where the z-update and x-update steps have the closed-form solutions via soft-thresholding and gradient method[16].

[14] Stephen Boyd et al. "Distributed Optimization and Statistical Learning via the Alternating Direction Method of Multipliers". In: *Foundations & Trends in Machine Learning* 3.1 (2011), pp. 1–122.

[15] Penghang Yin et al. "Minimization of ℓ_{1-2} for compressed sensing". In: *SIAM Journal on Scientific Computing* 37.1 (2015), A536–A563.

[16] Yin et al., "Minimization of ℓ_{1-2} for compressed sensing".

Two implementations

We have provided close-form expression of DCA and ADMM, here we will investigate two L_{1-2} implementations based on DCA and ADMM with distrinct execution order of the iterations 17 and 21.

- In the first scheme, also called DCA-L_{1-2}, the gradient y is updated after l^1_{max} inner iterations of ADMM within k^1_{max} outer iterations;
- whereas the gradient y is updated after every iteration of ADMM, x, z, w and y are updated simultaneously within l^2_{max} iterations, in the second scheme called ADMM-L_{1-2}.

DCA-L_{1-2}

Algorithm 1 DCA-L_{1-2} for seismic attenuation compensation

Input: A, b, λ, α, k^1_{max}, l^1_{max}.
Output: $x := x^k$.

Initialization: Set $x^0 := \mathbf{0}$, $w^0 := \mathbf{0}$, and $k := 0$.
for $k = 0 \cdots k^1_{max}$ **do**
  if $x = \mathbf{0}$ **then**
    $y^k = \mathbf{0}$;
  else
    $y^k = -\alpha\lambda \frac{x^k}{\|x^k\|_2}$;
  end if
  Initialization: Set $x^{k+1,0} := x^k$, $w^{k+1,0} := w^k$, and $l := 0$.
  for $l = 0 \cdots l^1_{max}$ **do**
    $z^{k+1,l+1} := \mathcal{S}\left(x^{k+1,l} + w^{k+1,l}/\rho, \lambda/\rho\right)$;
    $x^{k+1,l+1} := \left(A^T A + \rho I\right)^{-1}\left(A^T b - y^k + \rho z^{k+1,l+1} - w^{k+1,l}\right)$;
    $w^{k+1,l+1} := w^{k,l} + \left(x^{k+1,l+1} - z^{k+1,l+1}\right)$;
    Set $l := l + 1$.
  end for
  Output: $x^{k+1} := x^{k+1,l}$ and $w^{k+1} := w^{k+1,l}$.
  Set $k := k + 1$.
end for

Figure 5. The pseudo-code of DCA-L_{1-2}.

ADMM-L_{1-2}

Algorithm 2 ADMM-L_{1-2} for seismic attenuation compensation

Input: $A,\ b,\ \lambda,\ \alpha,\ l^2_{max}$.
Output: $x := x^l$.

Initialization: Set $x^0 := \mathbf{0}$, $w^0 := \mathbf{0}$, $y^0 := \mathbf{0}$ and $l := 0$.
for $l = 0 \cdots l^2_{max}$ **do**
  if $x^l = \mathbf{0}$ **then**
    $y^l = \mathbf{0}$;
  else
    $y^l = -\alpha\lambda \frac{x^l}{\|x^l\|_2}$;
  end if
  $z^{l+1} := \mathcal{S}\left(x^l + w^l/\rho, \lambda/\rho\right)$;
  $x^{l+1} := \left(A^T A + \rho I\right)^{-1}\left(A^T b - y^l + \rho z^{l+1} - w^l\right)$;
  $w^{l+1} := w^l + \left(x^{l+1} - z^{l+1}\right)$;
  Set $l := l + 1$.
end for

Figure 6. The pseudo-code of ADMM-L_{1-2}.

2D noise-free synthetic data

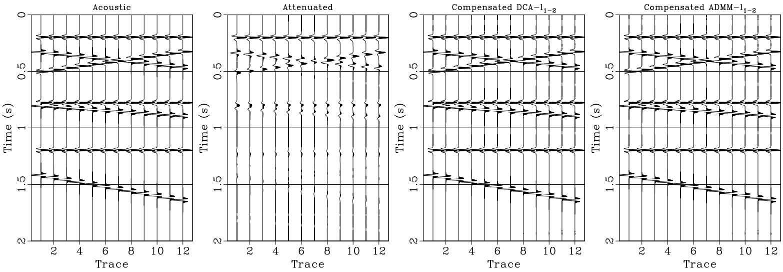

Figure 7. Seismic attenuation compensation on 2D noise-free synthetic data, (a) acoustic data, (b) attenuated data, (c) compensated data using DCA-L_{1-2} algorithm and (d) compensated data using ADMM-L_{1-2} algorithm.

2D noise-free synthetic data

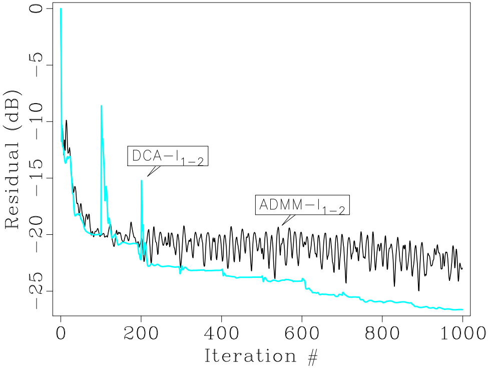

Figure 8. Comparison between DCA-L_{1-2} and ADMM-L_{1-2} in terms of residual errors versus iterations.

2D noisy synthetic data

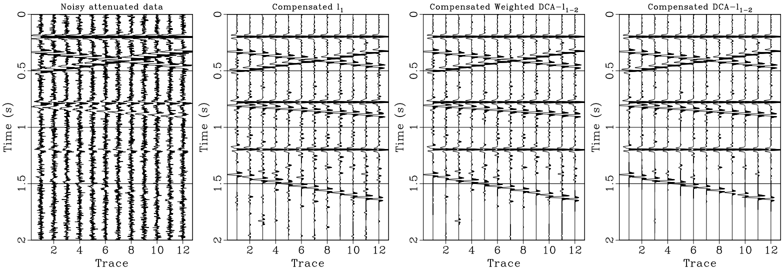

Figure 9. Seismic attenuation compensation on 2D noisy synthetic data, (a) noisy attenuated data, (b) compensated data using L_1 minimization (SNR=9.57), (c) compensated data using weighted DCA-$L_{1-\alpha 2}$ algorithm (where $\alpha = 0.5$, SNR=10.23) and (d) compensated data using DCA-L_{1-2} algorithm (SNR=10.77).

2D noisy synthetic data

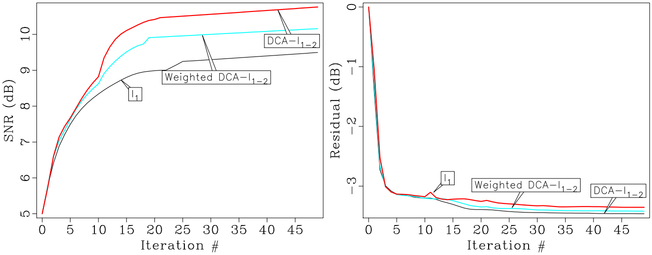

Figure 10. Comparison between L_1, weighted DCA-$L_{1-\alpha 2}$ and DCA-L_{1-2} in terms of (a) SNR versus iterations and (b) residual errors versus iterations.

2D field data

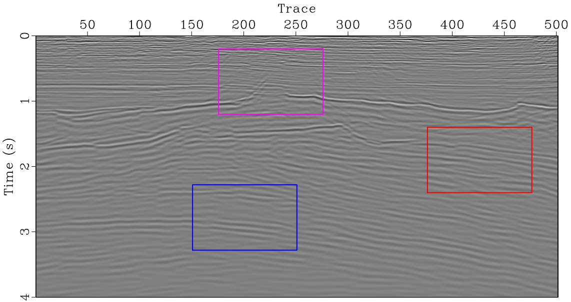

Figure 11. 2D original attenuated data.

2D field data

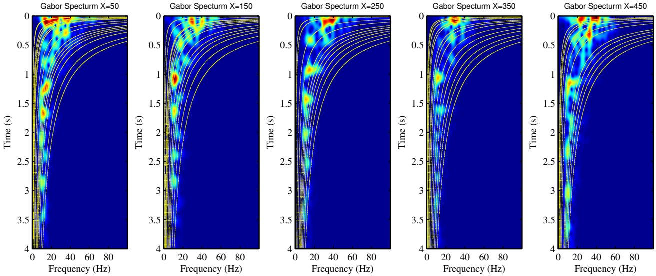

Figure 12. The Gabor spectra of five reference traces from original attenuated data.

2D field data

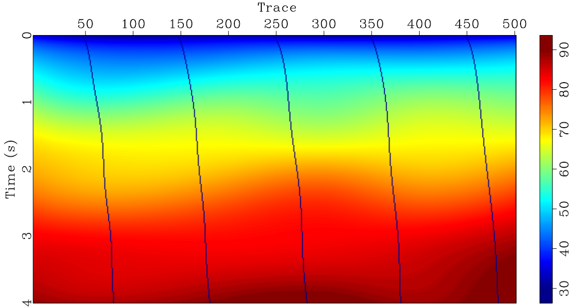

Figure 13. The estimated effective Q model from original attenuated data, which is obtained by horizontal interpolation from five reference Q curves.

2D field data

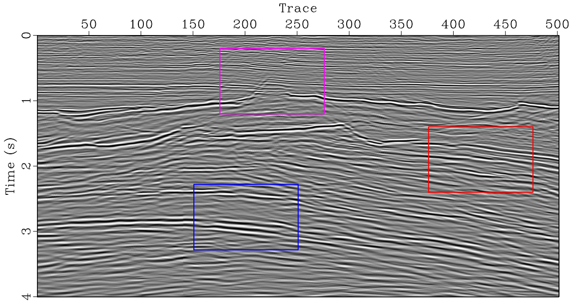

Figure 14. Compensated data using our peoposed L_{1-2} minimization.

2D field data

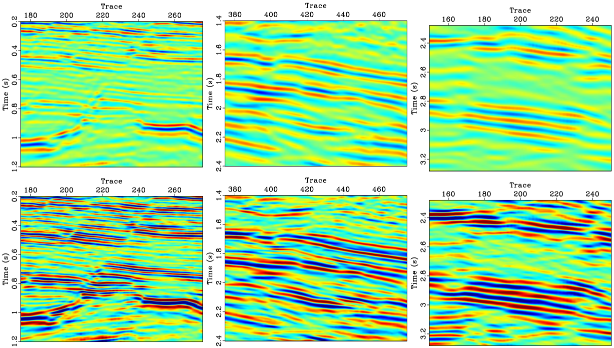

Figure 15. Zoomed view of the 2D field data, (top) original attenuated data from the boxes shown in Figure 11; (bottom) compensated data from the boxes shown in Figure 14.

2D field data

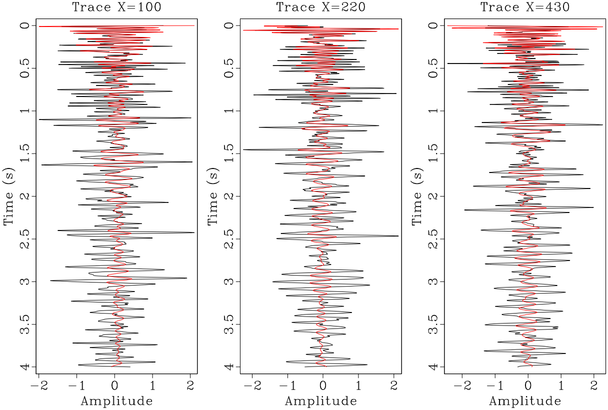

Figure 16. Comparison of compensation performance using three reference traces extracted from Figures 11 and 14 at (a) X=100, (b) X=220 and (c) X=430, respectively.

2D field data

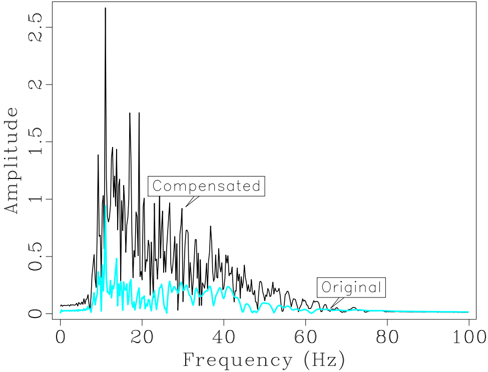

Figure 17. Comparison of the averaged spectra from the original data shown in Figure 11 and the compensated data shown in Figure 14.

3D field data

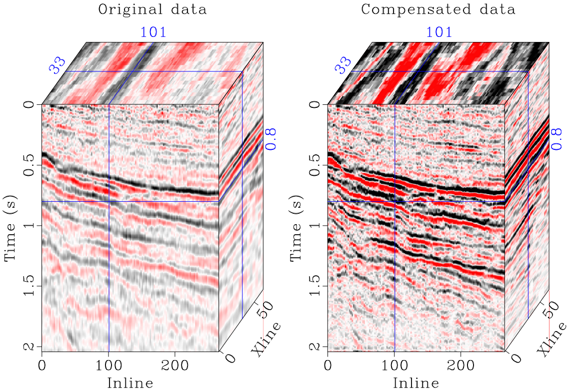

Figure 18. Seismic attenuation compensation on 3D field data, (left) original attenuated data and (right) compensated data using our peoposed L_{1-2} minimization.

3D field data

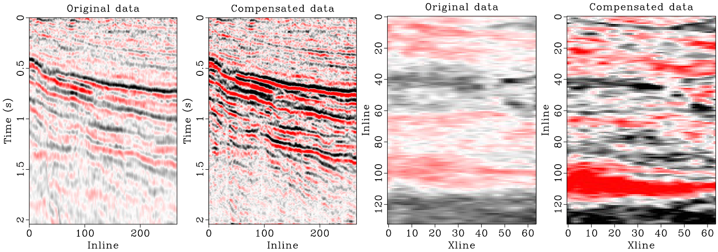

Figure 19. Comparison of compensation performance using corssline sections at X = 40 from (a) the original data shown in Figure 18a and (b) the compensated data shown in Figure 18b and time slices at $t = 1$s from (c) the original data shown in Figure 18a and (d) the compensated data shown in Figure 18b.

Wavelet dependence

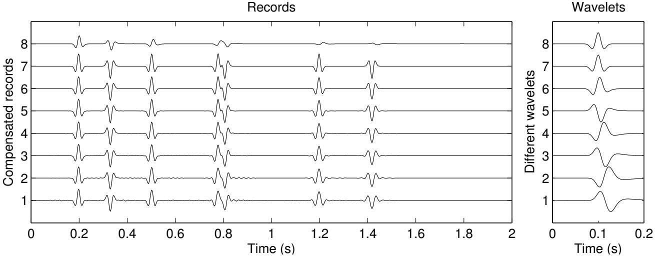

Figure 20. Seismic attenuation compensation using inaccurate wavelet, (a) the compensated 1D clean data and (b) their corresponding different wavelets.

Wavelet dependence

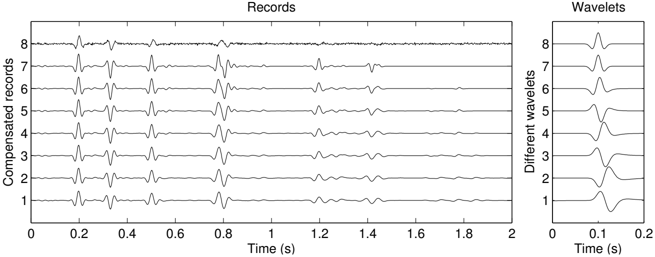

Figure 21. Seismic attenuation compensation using inaccurate wavelet, (a) the compensated 1D noisy data and (b) their corresponding different wavelets.

Parameter selection

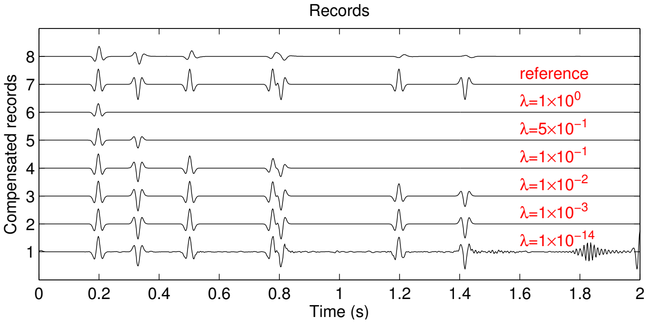

Figure 22. Seismic attenuation compensation using different balancing parameters λ tested on 1D clean data.

Parameter selection

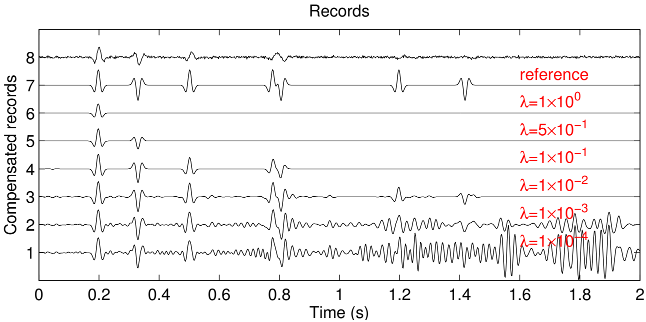

Figure 23. Seismic attenuation compensation using different balancing parameters λ tested on 1D noisy data.

Outline

- Motivation
- L_{1-2} minimization for seismic attenuation compensation
  - Nonstationary convolution model
  - Inversion-based compensation
  - Solver for L_{1-2} minimization
  - Examples
- Adaptive stabilization for Q-ARTM and Q-ERTM
  - Constant-Q wave equation and k-space Green's function
  - Adaptive stabilization
  - From viscoacoustic to viscoelastic
  - Examples
- High performance computing and code packages
  - Reproducible research
  - Architecture of cu$Q$-RTM code package
  - Speedup and scaling
- Summary

From temporal fractional derivatives to DFLs

Several researchers reformulated the temporal fractional derivatives into the decoupled fractional Laplacians (DFLs) using the smallness approximation and Euler's formula[17][18][19][20]. Considering the Fourier transform of the fractional temporal derivative of the wavefiled function $u(\mathbf{r}, t)$,

$$\mathcal{F}\left\{\frac{\partial^\alpha u(\mathbf{r}, t)}{\partial t^\alpha}\right\} = (i\omega)^\alpha U(k, \omega). \tag{22}$$

[17] W. Chen and S Holm. "Fractional Laplacian time-space models for linear and nonlinear lossy media exhibiting arbitrary frequency power-law dependency.". In: *Journal of the Acoustical Society of America* 115.4 (2004), pp. 1424–30.

[18] B. E. Treeby and B. T. Cox. "Modeling power law absorption and dispersion for acoustic propagation using the fractional Laplacian.". In: *Journal of the Acoustical Society of America* 127.5 (2010), pp. 2741–48.

[19] Jose M. Carcione. "A generalization of the Fourier pseudospectral method". In: *Geophysics* 75.6 (2010), A53–A56.

[20] Tieyuan Zhu and Jerry M. Harris. "Modeling acoustic wave propagation in heterogeneous attenuating media using decoupled fractional Laplacians". In: *Geophysics* 79.3 (2014), T105–T116.

From temporal fractional derivatives to DFLs

Using the smallness approximation $k_I \ll k_R$ $(k \approx \omega/c_0)$ and Euler's formula

$$\begin{aligned}(i\omega)^\alpha &= \cos\left(\frac{\pi\alpha}{2}\right)\omega^\alpha + (i\omega)\sin\left(\frac{\pi\alpha}{2}\right)\omega^{\alpha-1} \\ &\approx \cos\left(\frac{\pi\alpha}{2}\right)c_0^\alpha k^\alpha + (i\omega)\sin\left(\frac{\pi\alpha}{2}\right)c_0^{\alpha-1}k^{\alpha-1}.\end{aligned} \tag{23}$$

Using the definition of the fractional Laplacian

$$\mathcal{F}\{(-\nabla^2)^\alpha u(\mathbf{r},t)\} = k^{2\alpha}U(k,\omega). \tag{24}$$

General principle of Q-RTM

Constant-Q viscoacoustic wave equation with DFLs was firstly proposed by Zhu and Harris (2014) as follows[21]

$$\begin{cases} \frac{1}{c^2(\mathbf{x})}\frac{\partial^2 p}{\partial t^2}(\mathbf{x},t) - \eta(-\nabla^2)^{\gamma+1}p(\mathbf{x},t) - \tau\frac{\partial}{\partial t}(-\nabla^2)^{\gamma+1/2}p(\mathbf{x},t) = \delta(\mathbf{x}-\mathbf{x}_s)f(t), \\ p(\mathbf{x},t) = \frac{\partial p}{\partial t}(\mathbf{x},t) = 0, \qquad \mathbf{x}\in\Omega, t<0. \end{cases} \tag{25}$$

The coefficients of two fractional Laplacians are given by

$$\eta(\mathbf{x}) = -c_0^{2\gamma(\mathbf{x})}(\mathbf{x})\omega_0^{-2\gamma(\mathbf{x})}\cos(\pi\gamma(\mathbf{x})), \tag{26}$$

$$\tau(\mathbf{x}) = -c_0^{2\gamma(\mathbf{x})-1}(\mathbf{x})\omega_0^{-2\gamma(\mathbf{x})}\sin(\pi\gamma(\mathbf{x})). \tag{27}$$

[21] Zhu and Harris, "Modeling acoustic wave propagation in heterogeneous attenuating media using decoupled fractional Laplacians".

General principle of Q-RTM

Zhu et al. (2014) implemented Q-RTM applying the zero-lag crosscorrelation imaging condition[22]

$$I(\mathbf{x}) = \int_0^T p_s(\mathbf{x}, t) p_r(\mathbf{x}, t) dt, \tag{28}$$

where the source wavefield $p_s(\mathbf{x}, t)$ and receiver wavefield $p_r(\mathbf{x}, t)$ are compensated simultaneously.

$$\begin{cases} \frac{1}{c^2(\mathbf{x})} \frac{\partial^2 p_s}{\partial t^2}(\mathbf{x}, t) - \eta(-\nabla^2)^{\gamma+1} p_s(\mathbf{x}, t) + \tau \frac{\partial}{\partial t}(-\nabla^2)^{\gamma+1/2} p_s(\mathbf{x}, t) = \delta(\mathbf{x} - \mathbf{x}_s) f(t), \\ p_s(\mathbf{x}, t) = \frac{\partial p_s}{\partial t}(\mathbf{x}, t) = 0, \qquad \mathbf{x} \in \Omega, t < 0. \end{cases} \tag{29}$$

$$\begin{cases} \frac{1}{c^2(\mathbf{x})} \frac{\partial^2 p_r}{\partial t^2}(\mathbf{x}, t) - \eta(-\nabla^2)^{\gamma+1} p_r(\mathbf{x}, t) + \tau \frac{\partial}{\partial t}(-\nabla^2)^{\gamma+1/2} p_r(\mathbf{x}, t) = \delta(\mathbf{x} - \mathbf{x}_r) g(\mathbf{x}, T - t), \\ g(\mathbf{x}, t) = p(\mathbf{x}, t), \qquad \mathbf{x} \in \mathbf{x}_r, t \in [0, T], \end{cases} \tag{30}$$

[22] Zhu, Harris, and Biondi, "Q-compensated reverse-time migration".

The k-space Green's functions

The k-space Green's function of equation 25 can be obtained by enforcing a point source at time $t = t_0$ and at the location $\mathbf{x} = \mathbf{x}_s$ and then performing space-time Fourier transform, it yields frequency-wavenumber harmonic Green's function $G(\mathbf{k}, \omega)$, which is the solution of the following Helmholtz equation[23]

$$\left(\frac{\omega^2}{c^2} + \eta|\mathbf{k}|^{2\gamma+2} + i\omega\tau|\mathbf{k}|^{2\gamma+1}\right) G(\mathbf{k}, \omega) = \frac{1}{(2\pi)^{d+1}} e^{-i\omega t_0} e^{i\mathbf{k}\mathbf{x}_s}. \quad (31)$$

[23] Yufeng Wang et al. "Adaptive stabilization for Q-compensated reverse time migration". In: *Geophysics* 83.1 (2018), S15–S32.

The k-space Green's functions

Solving for frequency-wavenumber harmonic Green's function $G(\mathbf{k}, \omega)$ and then applying $d+1$ dimensional inverse Fourier transform, we have

$$G(\mathbf{x}, t) = \frac{c^2}{(2\pi)^{d+1}} \int_{-\infty}^{\infty} \int_{\mathbb{C}^d} h(\mathbf{k}, \omega) d\mathbf{k} d\omega, \tag{32}$$

where the integral kernel function is

$$h(\mathbf{k}, \omega) = \frac{e^{i\omega(t-t_0)} e^{-i\mathbf{k}(\mathbf{x}-\mathbf{x}_s)}}{\omega^2 + \eta|\mathbf{k}|^{2\gamma+2} c^2 + i\omega\tau|\mathbf{k}|^{2\gamma+1} c^2}. \tag{33}$$

The k-space Green's functions

The two singularities of this integral kernel function $h(\mathbf{k},\omega)$ can be obtained by solving ω for the following equation

$$\frac{\omega^2}{c^2} + \eta|\mathbf{k}|^{2\gamma+2} + i\omega\tau|\mathbf{k}|^{2\gamma+1} = 0. \tag{34}$$

The solutions of equation 34 are given by

$$\zeta_{1,2}(\mathbf{k}) = \pm\xi_1(\mathbf{k}) + i\xi_2(\mathbf{k}), \tag{35}$$

where

$$\xi_1(\mathbf{k}) = \sqrt{-\tau^2c^4|\mathbf{k}|^{4\gamma+2} - 4\eta c^2|\mathbf{k}|^{2\gamma+2}}/2, \tag{36}$$

$$\xi_2(\mathbf{k}) = -\tau c^2|\mathbf{k}|^{2\gamma+1}/2. \tag{37}$$

The k-space Green's functions

According to Cauchy's residue theorem, we deduce the analytical integration of $h(\mathbf{k},\omega)$ with respect to ω

$$\int_{-\infty}^{\infty} h(\mathbf{k},\omega)d(\omega) = 2\pi \frac{\sin(\xi_1(\mathbf{k})t)e^{-\xi_2(\mathbf{k})t}}{\xi_1(\mathbf{k})}. \tag{38}$$

Therefore this Green's function can be further expressed as

$$G(\mathbf{x},t) = \frac{c^2}{(2\pi)^d} \int_{\mathbb{C}^d} \Gamma_{att}(\mathbf{k},t)d\mathbf{k}, \tag{39}$$

where the attenuated time propagator $\Gamma_{att}(\mathbf{k},t)$ is given by

$$\Gamma_{att}(\mathbf{k},t) = \frac{\sin(\xi_1(\mathbf{k})t)e^{-\xi_2(\mathbf{k})t}}{\xi_1(\mathbf{k})}. \tag{40}$$

The k-space Green's functions

The Green's function for compensated equations 29 and 30 can be derived by reversing the absorption-related term τ in sign but leaving the other term η unchanged. The compensated time propagator $\Gamma_{comp}(\mathbf{k}, t)$ is

$$\Gamma_{comp}(\mathbf{k}, t) = \frac{\sin(\xi_1(\mathbf{k})t)e^{\xi_2(\mathbf{k})t}}{\xi_1(\mathbf{k})}. \tag{41}$$

For lossless media, we have

$$\Gamma_{aco}(\mathbf{k}, t) = \Gamma_{comp}(\mathbf{k}, t) = \Gamma_{att}(\mathbf{k}, t) = \frac{\sin(c_0|\mathbf{k}|t)}{c_0|\mathbf{k}|}. \tag{42}$$

The k-space Green's functions

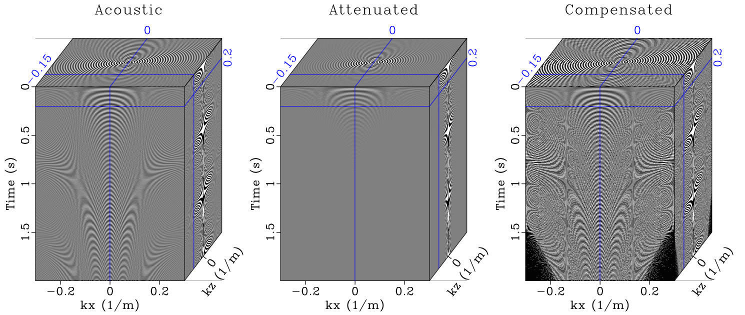

Figure 24. Time propagators of k-space Green's functions for: (a) acoustic wave equation, (b) constant-Q wave equation, (c) compensated constant-Q wave equation.

Adaptive stabilization

Wang (2006) proposed a stabilized amplitude-compensated operator for inverse Q filtering[24].

$$\Lambda(\tau,\omega) = \frac{\beta(\tau,\omega)}{\beta^2(\tau,\omega)+\sigma^2}, \tag{43}$$

where $\beta(\tau,\omega)$ is an amplitude-attenuated operator and σ^2 is the stabilization factor. We propose a similar adaptive stabilization for Q-RTM by defining the amplitude-attenuated operator

$$\beta(\mathbf{k},t) = e^{-\xi_2(\mathbf{k})t}, \tag{44}$$

and stabilized amplitude-compensated operator

$$\Lambda(\mathbf{k},t) = \frac{\beta(\mathbf{k},t)}{\beta^2(\mathbf{k},t)+\sigma^2} = \frac{e^{\xi_2(\mathbf{k})t}}{1+\sigma^2 e^{2\xi_2(\mathbf{k})t}}. \tag{45}$$

[24] Yanghua Wang. "Inverse Q-filter for seismic resolution enhancement". In: *Geophysics* 71.3 (2006), pp. V51–V60.

Adaptive stabilization

In fact, the compensation operator $e^{\xi_2(\mathbf{k})t}$ has been embodied in equations 29 and 30, therefore we merely need to modify the Q-RTM scheme by introducing a stabilization operator given as

$$S(\mathbf{k},t) = \frac{1}{1+\sigma^2 e^{2\xi_2(\mathbf{k})t}}. \tag{46}$$

The attenuation and compensation effects in Q-RTM are considered to be accumulated from the starting time to the current time, and thus we need to perform stabilization at every time step Δt.

$$\prod_{l=1}^{n} s(\mathbf{k}, l\Delta t) = S(\mathbf{k}, n\Delta t). \tag{47}$$

Adaptive stabilization

The final form of our proposed stabilization operator can be given by

$$s(\mathbf{k}, l\Delta t) = \begin{cases} \dfrac{1}{1+\sigma^2 e^{2\xi_2(\mathbf{k})\Delta t}}, & l = 1, \\ \dfrac{1+\sigma^2 e^{2\xi_2(l-1)\Delta t}}{1+\sigma^2 e^{2\xi_2 l\Delta t}}, & l = 2, 3, \ldots, n. \end{cases} \tag{48}$$

Adaptive stabilization

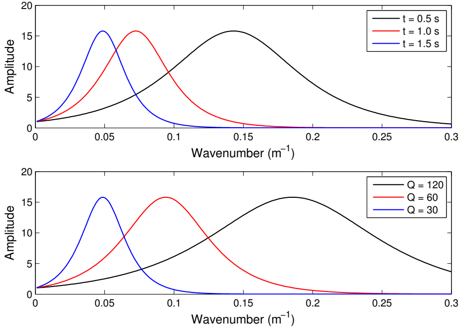

Figure 25. The stabilized compensation coefficients $\Lambda(\mathbf{k}, t)$ varying with: (a) different traveltime $t = 0.5$ s, 1.0 s and 1.5 ($Q = 30$ and $\sigma^2 = 0.1\%$), (b) different quality factor $Q = 120, 60$ and 30 ($t = 1.5$ and $\sigma^2 = 0.1\%$).

Adaptive stabilization

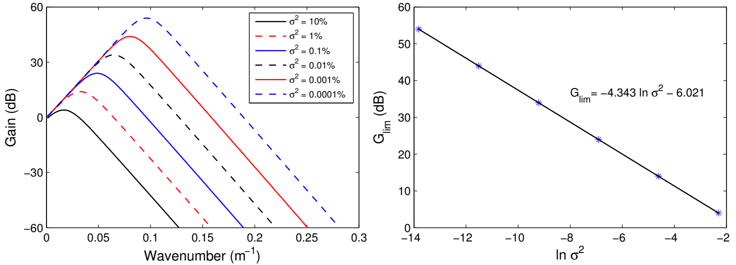

Figure 26. (left) The stabilized compensation curves $\Lambda(\mathbf{k}, t)$ (in decibels) varying with a series of stabilization factors σ^2 (from 10% to 0.0001%), (right) linear fitting for gain limit G_{lim} varying with $\ln\sigma^2$.

Adaptive stabilization vs. low-pass filtering

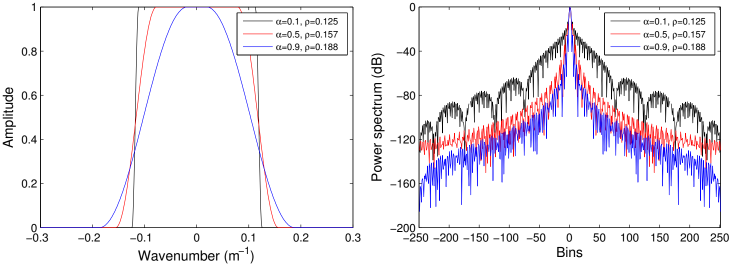

Figure 27. Tukey windows and their power spectra with different taper ratios α and cut-off parameters ρ: (left) Tukey windows and (right) their power spectra.

Adaptive stabilization vs. low-pass filtering

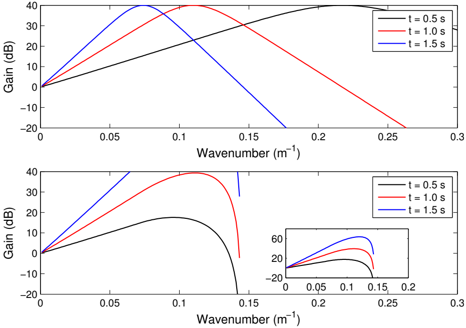

Figure 28. The compensation curves (in decibels) at different traveltime $t = 0.5$ s, 1.0 s and 1.5 s, which is stabilized by (a) adaptive stabilization ($\sigma^2 = 0.0025\%$) and (b) low-pass Tukey filtering ($\rho = 0.14\ \mathrm{m}^{-1}$).

Adaptive stabilization vs. low-pass filtering

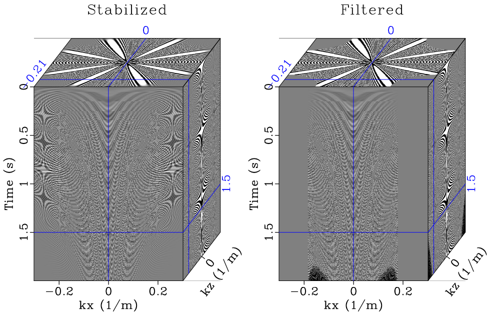

Figure 29. The compensated time propagators stabilized by (a) adaptive stabilization ($\sigma^2 = 2.5 \times 10^{-7}$) and (b) low-pass Tukey filtering ($\rho = 0.16\ \mathrm{m}^{-1}$). We clip the same amplitude value for these two figures.

Viscoelastic wave equation with DFLs

The constant-Q viscoelastic wave equation with DFLs in a first-order matrix form:

$$\partial_t \mathbf{u}^\diamond = \mathbf{H}\mathbf{u}^\diamond + \mathbf{f}, \tag{49}$$

where $\mathbf{u}^\diamond = (v_x, v_z, \sigma_{xx}, \sigma_{zz}, \sigma_{xz})^T$ is the 5×1 unknown field array, $\mathbf{f} = (f_x, f_z, 0, 0, 0)^T$ is the 5×1 source array, and

$$\mathbf{H} = \begin{pmatrix} 0 & 0 & 1/\rho\partial_x & 0 & 1/\rho\partial_z \\ 0 & 0 & 0 & 1/\rho\partial_z & 1/\rho\partial_x \\ (\overline{\boldsymbol{\lambda}} + 2\overline{\boldsymbol{\mu}})\partial_x & \overline{\boldsymbol{\lambda}}\partial_z & 0 & 0 & 0 \\ \overline{\boldsymbol{\lambda}}\partial_x & (\overline{\boldsymbol{\lambda}} + 2\overline{\boldsymbol{\mu}})\partial_z & 0 & 0 & 0 \\ \overline{\boldsymbol{\mu}}\partial_z & \overline{\boldsymbol{\mu}}\partial_x & 0 & 0 & 0 \end{pmatrix} \tag{50}$$

Viscoelastic wave equation with DFLs

$\overline{\boldsymbol{\lambda}}$ and $\overline{\boldsymbol{\mu}}$ in this operator represent generalized Lamé coefficients under viscoelastic case, which can be expressed as

$$\overline{\boldsymbol{\lambda}} + 2\overline{\boldsymbol{\mu}} = \eta_p \mathbf{D}_p + \tau_p \mathbf{A}_p \partial_t, \tag{51}$$

$$\overline{\boldsymbol{\mu}} = \eta_s \mathbf{D}_s + \tau_s \mathbf{A}_s \partial_t, \tag{52}$$

$$\overline{\boldsymbol{\lambda}} = \left(\eta_p \mathbf{D}_p + \tau_p \mathbf{A}_p \partial_t\right) - 2\left(\eta_s \mathbf{D}_s + \tau_s \mathbf{A}_s \partial_t\right). \tag{53}$$

There are two fractional Laplacians in these coefficients, i.e.,

$$\mathbf{D}_m = (-\nabla^2)^{\gamma_m}, \qquad \mathbf{A}_m = (-\nabla^2)^{\gamma_m - 1/2}, \qquad m = p, s, \tag{54}$$

which are respectively responsible for phase velocity dispersion and amplitude attenuation.

Viscoelastic wavefield decomposition

We conduct P- and S-wavefield decomposition by introducing the P-wave stress variable σ_p and S-wave stress variable σ_s.

$$\partial_t \mathbf{u}^\circ = \mathbf{W}\mathbf{u}^\bullet, \tag{55}$$

where $\mathbf{u}^\circ = (\sigma_p, v_{xp}, v_{zp}, \sigma_s, v_{xs}, v_{zs})^T$ is the 6×1 decomposed wavefield array, $\mathbf{u}^\bullet = (v_x, v_z, \sigma_p, \sigma_s)^T$ is the 4×1 hybrid wavefield array, and

$$\mathbf{W} = \begin{pmatrix} (\overline{\boldsymbol{\lambda}} + 2\overline{\boldsymbol{\mu}})\partial_x & \overline{\boldsymbol{\lambda}}\partial_z & 0 & 0 \\ 0 & 0 & 1/\rho\partial_x & 0 \\ 0 & 0 & 1/\rho\partial_z & 0 \\ \overline{\boldsymbol{\mu}}\partial_z & -\overline{\boldsymbol{\mu}}\partial_x & 0 & 0 \\ 0 & 0 & 0 & 1/\rho\partial_z \\ 0 & 0 & 0 & -1/\rho\partial_x \end{pmatrix}. \tag{56}$$

Viscoelastic wavefield decomposition

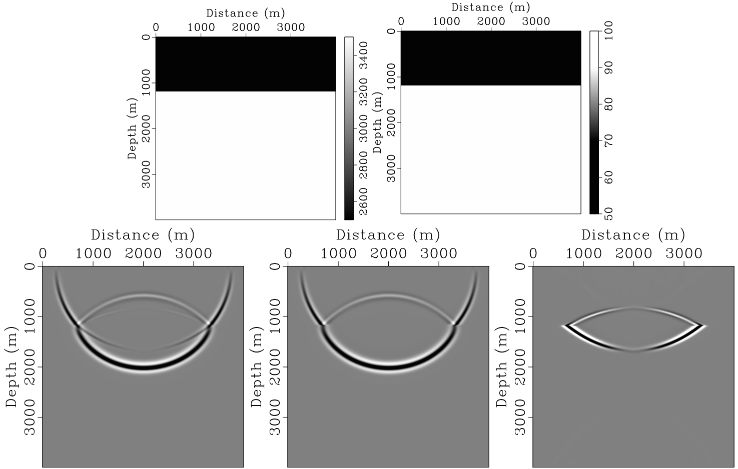

Viscoelastic imaging condition

We adopt source-normalized crosscorrelation imaging conditions in the inner product form for vector-based viscoelastic imaging.

$$
\begin{aligned}
I_{pp}(\mathbf{x}) &= \frac{\int_0^T \mathbf{v}_p^{S^a}(\mathbf{x},t)\cdot \mathbf{v}_p^{R^c}(\mathbf{x},t)}{\int_0^T \mathbf{v}_p^{S^a}(\mathbf{x},t)\cdot \mathbf{v}_p^{S^a}(\mathbf{x},t)}dt, \\
I_{ps}(\mathbf{x}) &= \frac{\int_0^T \mathbf{v}_p^{S^a}(\mathbf{x},t)\cdot \mathbf{v}_s^{R^c}(\mathbf{x},t)}{\int_0^T \mathbf{v}_p^{S^a}(\mathbf{x},t)\cdot \mathbf{v}_p^{S^a}(\mathbf{x},t)}dt.
\end{aligned} \tag{57}
$$

Mode-dependent adaptive stabilization

In homogeneous media, the second-order viscoelastic wave equation has the following form:

$$\rho\frac{\partial^2\mathbf{u}}{\partial t^2} - (\eta_p\mathbf{D}_p + \tau_p\mathbf{A}_p\partial_t)\nabla(\nabla\cdot\mathbf{u}) + (\eta_s\mathbf{D}_s + \tau_s\mathbf{A}_s\partial_t)\nabla\times(\nabla\times\mathbf{u}) = \mathbf{0}, \tag{58}$$

According to Helmholtz's theorems, the vector equation 58 can be split into P- and S-wave propagation:

$$\rho\frac{\partial^2\mathbf{u}_p}{\partial t^2} - (\eta_p\mathbf{D}_p + \tau_p\mathbf{A}_p\partial_t)\nabla(\nabla\cdot\mathbf{u}_p) = 0, \tag{59}$$

and

$$\rho\frac{\partial^2\mathbf{u}_s}{\partial t^2} + (\eta_s\mathbf{D}_s + \tau_s\mathbf{A}_s\partial_t)\nabla\times(\nabla\times\mathbf{u}_s) = \mathbf{0}. \tag{60}$$

Mode-dependent adaptive stabilization

The P- and S-wave modes satisfy an unified form. Therefore, the mode-dependent adaptive stabilization can be given as

$$\Upsilon_m(\mathbf{k}, l\Delta t) = \begin{cases} \dfrac{1}{1+\sigma^2 e^{2\xi_m(\mathbf{k})\Delta t}}, & l = 1, \\ \dfrac{1+\sigma^2 e^{2\xi_m(l-1)\Delta t}}{1+\sigma^2 e^{2\xi_m(\mathbf{k})l\Delta t}}, & l = 2, 3, \ldots, n, \end{cases} \tag{61}$$

Mode-dependent adaptive stabilization

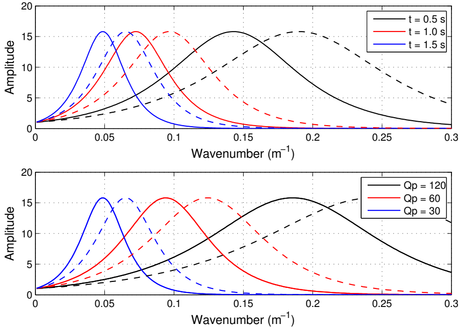

Figure 30. The stabilized compensation coefficients $\Lambda(\mathbf{k}, t)$ varying with: (a) different travel time $t = 0.5$ s, 1.0 s, and 1.5 ($Q_p = 30$ and $\sigma^2 = 0.1\%$), (b) different quality factor $Q_p = 120, 60,$ and 30 ($t = 1.5$ and $\sigma^2 = 0.1\%$), where the solid lines represent a P-wave and dash lines an S-wave. For simplicity, we set $c_p/c_s = 1.7$ and $Q_p/Q_s = 1.3$ for this synthetic example.

Synthetic test: Q-ARTM

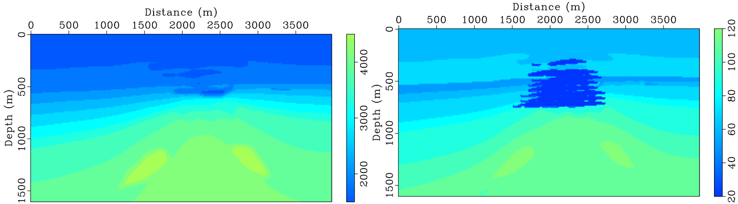

Figure 31. (left) Velocity and (right) Q of BP gas chimney model, which contains a high-attenuation gas chimney exhibiting an extreme attenuating property with $Q = 20$.

Synthetic test: Q-ARTM

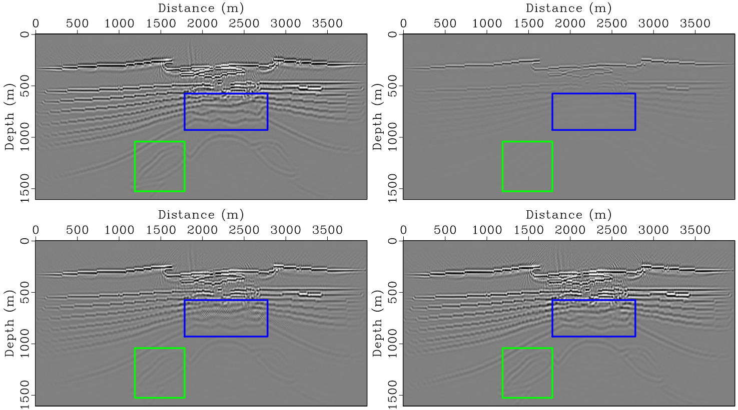

Figure 32. Migrated images obtained using (a) acoustic RTM, (b) viscoacoustic RTM without compensation, (c) low-pass filtered Q-RTM and (d) adaptively stabilized Q-RTM.

Field data application: Q-ARTM

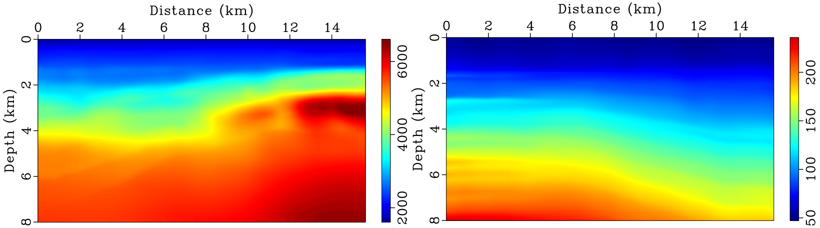

Figure 33. (top) Velocity and (bottom) Q models for field data.

Field data application: Q-ARTM

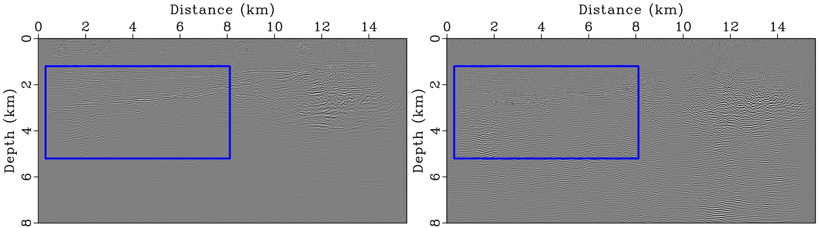

Figure 34. Migrated images of the field data using (top) conventional RTM from viscoacoustic media without compensation, (bottom) Q-RTM.

Field data application: Q-ARTM

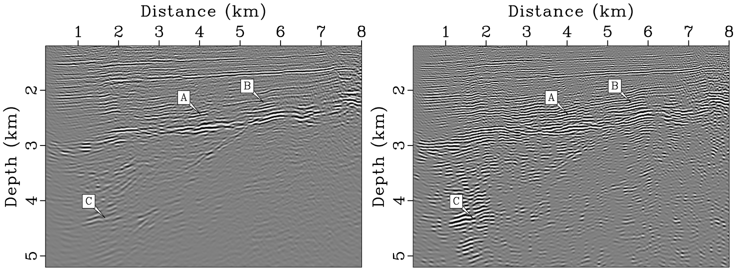

Figure 35. Zoom view of the images shown in the boxs in Figure 34.

Synthetic test: Q-ERTM

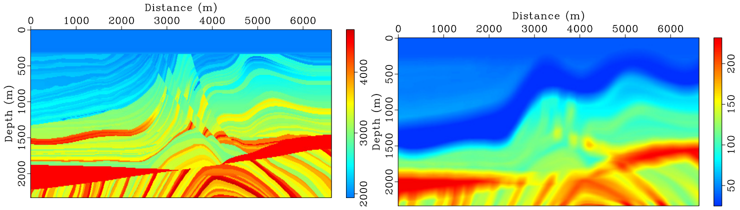

Figure 36. (left) P-wave velocity and (right) Q_p of the Marmousi model, and S-wave velocity c_s and S-wave quality factor Q_s are simply obtained by setting $c_p/c_s = 1.7$ and $Q_p/Q_s = 1.3$.

Synthetic test: Q-ERTM

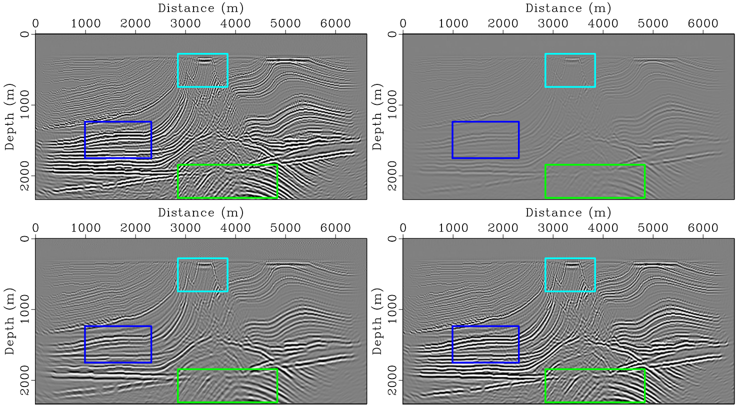

Figure 37. Migrated PP images of the Marmousi model obtained by (a) elastic RTM, (b) viscoelastic RTM without compensation, (c) low-pass filtered Q-ERTM, and (d) adaptively stabilized Q-ERTM.

Synthetic test: Q-ERTM

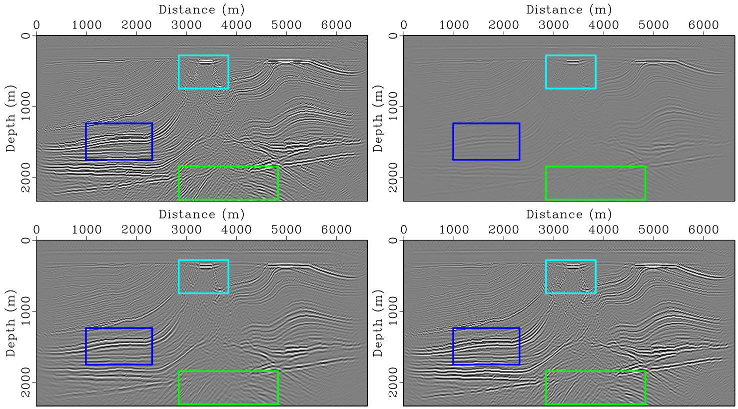

Figure 38. Migrated PS images of the Marmousi model obtained by (a) elastic RTM, (b) viscoelastic RTM without compensation, (c) low-pass filtered Q-ERTM, and (d) adaptively stabilized Q-ERTM.

Synthetic test: Q-ERTM

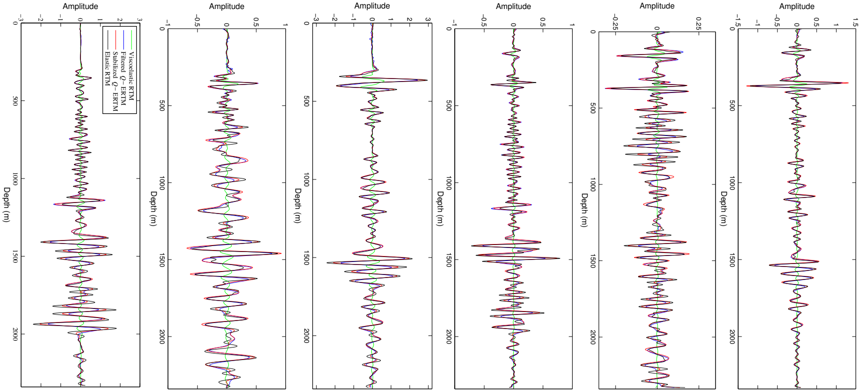

Figure 39. Migrated traces selected arbitrarily from PP imaging results at three distances of (a)(d) 1.6 km, (b)(e) 3.8 km and (c)(f) 5.2 km.

Synthetic test: Q-ERTM

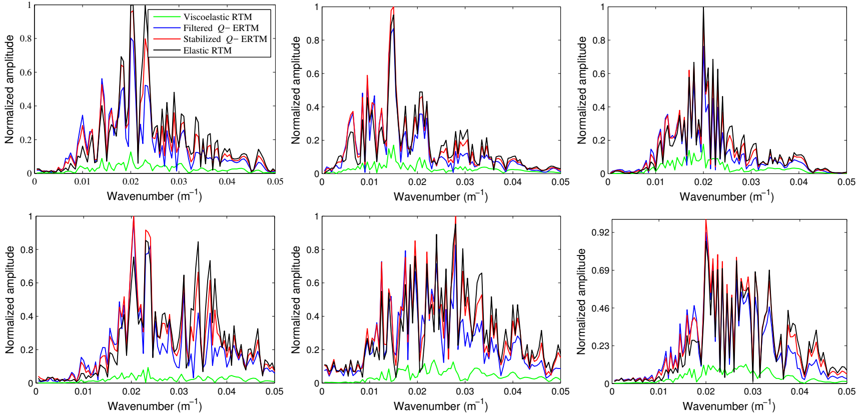

Figure 40. Wavenumber spectra corresponding to the traces shown in Figure 39.

Field data application: Q-ERTM

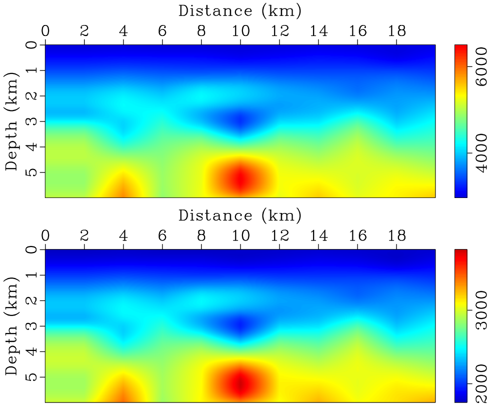

Figure 41. (top) P-wave velocity and (bottom) S-wave velocity of the field data.

Field data application: Q-ERTM

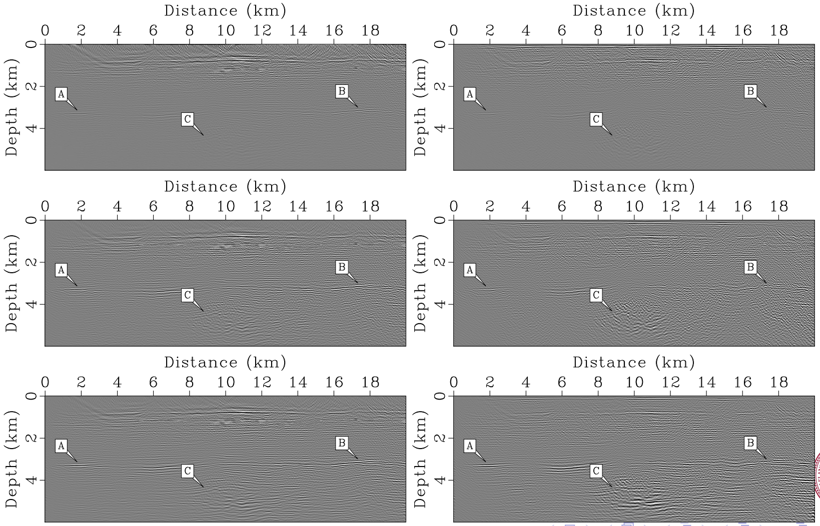

Field data application: Q-ERTM

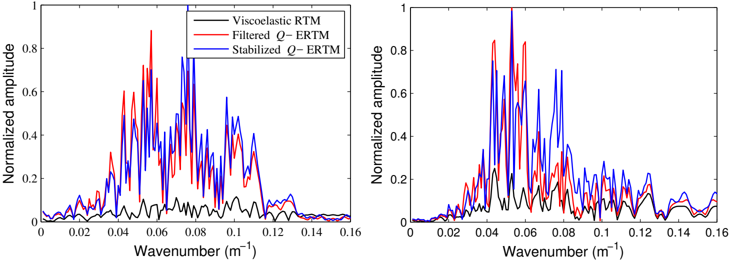

Figure 43. Wavenumber spectra of the reference traces selected from migrated images (X = 6 km), where the black lines stand for the spectra of the the non-compensated traces, the red lines for the conventional filtered ones, and the blue lines for the adaptively satabilized ones.

Outline

Motivation
L_{1-2} minimization for seismic attenuation compensation
- Nonstationary convolution model
- Inversion-based compensation
- Solver for L_{1-2} minimization
- Examples

Adaptive stabilization for Q-ARTM and Q-ERTM
- Constant-Q wave equation and k-space Green's function
- Adaptive stabilization
- From viscoacoustic to viscoelastic
- Examples

High performance computing and code packages
- Reproducible research
- Architecture of cu$Q$-RTM code package
- Speedup and scaling

Summary

Reproducible Research

- Claerbout's principle - an article about computational science in a scientific publication is not the scholarship itself, it is merely advertising of the scholarship. The actual scholarship is the complete software development environment and the complete set of instructions which generated the figures. (SEPlib)
- Dave Donoho's approach was to make sure that the details underlying the datasets, simulations, figures and tables were all expressed uniformly in the standard language and computing environment Matlab, and made available on the internet, so that interested parties could reproduce the calculations underlying that paper. (WaveLab)
- Sergey Fomel et. al. developed Madagascar: open-source software project for multidimensional data analysis and reproducible computational experiments. (Madagascar)

Benefits from Reproducible Research

- If everyone in a research team knows that everything they do is going to someday be published for reproducibility, they will behave differently and will do better work.
- It is a fundamental fact that in striving for reproducibility, we are producing code for the use of strangers. Developing for a stranger means avoiding reliance on this soft, transient knowledge; more specifically, codifying that knowledge objectively and reproducibly.
- There are some very important strangers in our lives: our co-authors, our students and future employers.
- More citation, more attention and more influence.

Architecture of cu$Q$-RTM code package

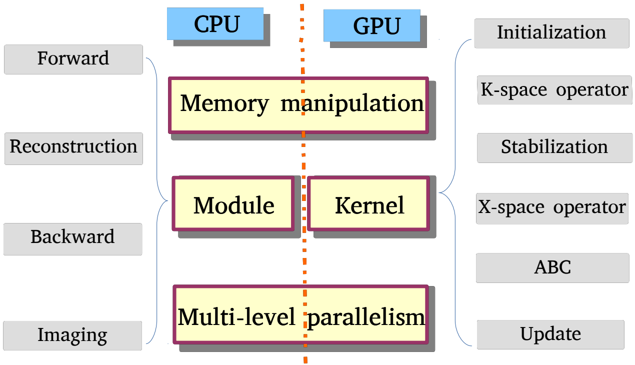

Figure 44. The architecture of the cu$Q$-RTM code package. The "living" package is available from GitHub at `https://github.com/Geophysics-OpenSource/cuQRTM`[25]

[25] Yufeng Wang et al. "CuQ-RTM: A CUDA-based code package for stable and efficient Q-compensated RTM". In: *Geophysics* 84.1 (2018), pp. 1–69.

Speedup and scaling

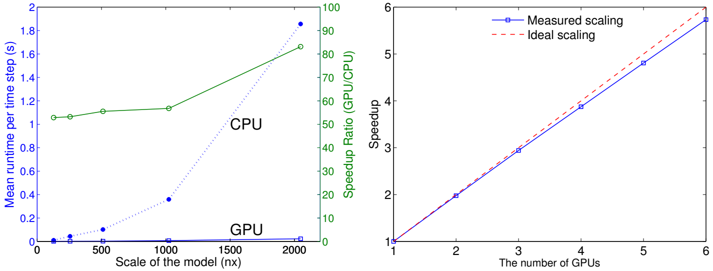

Figure 45. Speedup and scaling test of the cu$Q$-RTM code package.

Outline

Motivation
L_{1-2} minimization for seismic attenuation compensation
- Nonstationary convolution model
- Inversion-based compensation
- Solver for L_{1-2} minimization
- Examples

Adaptive stabilization for Q-ARTM and Q-ERTM
- Constant-Q wave equation and k-space Green's function
- Adaptive stabilization
- From viscoacoustic to viscoelastic
- Examples

High performance computing and code packages
- Reproducible research
- Architecture of cu$Q$-RTM code package
- Speedup and scaling

Summary

Summary

- Seismic attenuation compensation is an important method to enhance signal resolution and fidelity, which can be performed on either prestack (Q-RTM) or poststack data (L_{1-2} minimization).
- Compared to conventional L_1 metric, our proposed L_{1-2} penalty has potential to recover exact sparse reflectivity series from noisy attenuated seismograms (kernel matrix is severely ill-conditioned).
- Compared to conventional low-pass filtering, our proposed stabilization scheme exhibits superior properties of time-variance and Q-dependence.
- We present a CUDA-based code package named cu$Q$-RTM, which aims to achieve an efficient, storage-saving and stable Q-RTM.

Rethink of the motivation

My current work is mainly motivated by the following open problems:

1. What is the most foundamental governing equation that can well explain wave propagation in attenuating media? How to reach a reconciliation of experimentally established frequency power law and physically based mechanical models?
2. What is the physical and mathematical connections among different attenuation models? how and why does the increasingly investigated fractional attenuation model work?
3. How can we effectively compensate the subsurface Q filtering effects during prestack seismic migration or poststack seismic profile processing?
4. What can we learn from such an intrinsic attenuation of the subsurface? how does it reflect rock physics properties, physical processes at play in earth?

Some perspectives

- All attenuation models are either based on experimental observation or mathematical (mechanical) approximation, there are many criterions to determine which model should be used? for example, experimentally fit, physically clear, mathematically concise, computationally efficient. Personally, I prefer to fractional models due to its concise parameterization and ability to model frequency-dependent attenuation over a wide band.

Some perspectives

- Fractional models as a generalization of classical models have the ability to characterize weak frequency-dependent (frequency power-law) seismic attenuation, which can be represented by classical elements with the number of units tends to infinity. Fractional model is not merely an empirical generalization of classical model, it may provide more fundamental explanation for dynamic system. More attention should be paied to this area from physics, engineering and mathematics communities.

Some perspectives

- Attenuation compensation in geophysics can be roughly classified into two categories: seismic record-based compensation and propagation-based compensation. I propose a nearly unbiased approximation of the vector sparsity, denoted as L_{1-2} minimization, for exact and stable seismic attenuation compensation. I develop an adaptive stabilization scheme for Q-ARTM and Q-ERTM, which exhibits the superior properties of time-variance and Q-dependence over conventional low-pass filtering.

Some perspectives

- Apart from compensating Q effects, we may expect to obtain some reservoir and geological information from attenuation and to better understand the physical processes at play in earth. The one thing I am sure is that attenuation of wave propagation is a wide scientific problem and involves a rich body of applications from seismic exploration, seismology, and material science. I would devote more attention to this area during my postdoctoral research.

References:

Ma, Tian-Hui, Yifei Lou, and Ting-Zhu Huang. "Truncated l_1-2 Models for Sparse Recovery and Rank Minimization". In: *SIAM Journal on Imaging Sciences* 10.3 (2017), pp. 1346–1380.

Candes, Emmanuel J, Michael B Wakin, and Stephen P Boyd. "Enhancing sparsity by reweighted ℓ_1 minimization". In: *Journal of Fourier analysis and applications* 14.5 (2008), pp. 877–905.

Zhang, Yu, Po Zhang, and Houzhu Zhang. "Compensating for visco-acoustic effects in reverse-time migration". In: *SEG expanded abstracts: 80th Annual international meeting*. 2010, pp. 3160–3164.

- Zhu, Tieyuan, Jerry M. Harris, and Biondo Biondi. "Q-compensated reverse-time migration". In: *Geophysics* 79.3 (2014), S77–S87.
- Kolsky, H. "LXXI. The propagation of stress pulses in viscoelastic solids". In: *Philosophical magazine* 1.8 (1956), pp. 693–710.
- Futterman, Walter I. "Dispersive body waves". In: *Journal of Geophysical research* 67.13 (1962), pp. 5279–5291.
- Wang, Yanghua and Jian Guo. "Modified Kolsky model for seismic attenuation and dispersion". In: *Journal of Geophysics & Engineering* 1.3 (2004), p. 187.
- Candes, Emmanuel J and Terence Tao. "Decoding by linear programming". In: *IEEE transactions on information theory* 51.12 (2005), pp. 4203–4215.

- Bandeira, Afonso S. et al. "Certifying the Restricted Isometry Property is Hard". In: *IEEE Transactions on Information Theory* 59.6 (2013), pp. 3448–3450.
- Donoho, D. L. and X. Huo. "Uncertainty principles and ideal atomic decomposition". In: *IEEE Transactions on Information Theory* 47.7 (2002), pp. 2845–2862.
- Wang, Yufeng et al. "L1-2 minimization for exact and stable seismic attenuation compensation". In: *Geophysical Journal International* 213.3 (2018), pp. 1629–1646.
- Lou, Yifei, Stanley Osher, and Jack Xin. "Computational Aspects of Constrained L1-L2 Minimization for Compressive Sensing". In: *Petroleum Science & Technology* 23.1 (2015), pp. 47–54.

Tao, Pham Dinh and Le Thi Hoai An. "A DC optimization algorithm for solving the trust-region subproblem". In: *SIAM Journal on Optimization* 8.2 (1998), pp. 476–505.

Boyd, Stephen et al. "Distributed Optimization and Statistical Learning via the Alternating Direction Method of Multipliers". In: *Foundations & Trends in Machine Learning* 3.1 (2011), pp. 1–122.

Yin, Penghang et al. "Minimization of ℓ_{1-2} for compressed sensing". In: *SIAM Journal on Scientific Computing* 37.1 (2015), A536–A563.

Chen, W. and S Holm. "Fractional Laplacian time-space models for linear and nonlinear lossy media exhibiting arbitrary frequency power-law dependency.". In: *Journal of the Acoustical Society of America* 115.4 (2004), pp. 1424–30.

Treeby, B. E. and B. T. Cox. "Modeling power law absorption and dispersion for acoustic propagation using the fractional Laplacian.". In: *Journal of the Acoustical Society of America* 127.5 (2010), pp. 2741–48.

Carcione, Jose M. "A generalization of the Fourier pseudospectral method". In: *Geophysics* 75.6 (2010), A53–A56.

Zhu, Tieyuan and Jerry M. Harris. "Modeling acoustic wave propagation in heterogeneous attenuating media using decoupled fractional Laplacians". In: *Geophysics* 79.3 (2014), T105–T116.

Wang, Yufeng et al. "Adaptive stabilization for Q-compensated reverse time migration". In: *Geophysics* 83.1 (2018), S15–S32.

Wang, Yanghua. "Inverse Q-filter for seismic resolution enhancement". In: *Geophysics* 71.3 (2006), pp. V51–V60.

Wang, Yufeng et al. "CuQ-RTM: A CUDA-based code package for stable and efficient Q-compensated RTM". In: *Geophysics* 84.1 (2018), pp. 1–69.

Thank you!